

Density functional studies of defects and defect-related luminescence in Mg_3N_2 Xiuli Yang,¹ Rumeng Zhao,¹ Yu-Hang Ji,¹ Hongliang Shi^{1,*} and Mao-Hua Du^{2,†}¹Department of Physics, Beihang University, Beijing 100191, China²Materials Science and Technology Division, Oak Ridge National Laboratory, Oak Ridge, Tennessee 37831, USA

(Received 5 December 2019; revised manuscript received 29 May 2020; accepted 8 June 2020; published 19 June 2020)

Mg_3N_2 is a promising material for light-emitting-diode applications. However, the microscopic origin of the broad yellow photoluminescence in Mg_3N_2 remains unknown. Here, defect properties and defect-related optical transitions are investigated based on the hybrid functional calculation. Our results show that the nitrogen vacancy introduces multiple localized defect states within the band gap, which play a dominant role in luminescent properties of Mg_3N_2 . Common impurities like hydrogen, oxygen, and carbon and their complexes with native defects are also studied. Compared with isolated V_{Mg} , $V_{\text{Mg}}\text{-H}$ and $V_{\text{Mg}}\text{-O}_\text{N}$ complexes have shallower transition levels. Our calculated optical excitation and emission peaks associated with isolated V_N are in good agreement with those observed in experiments. In addition, the impurity C_N is also a potential source for the observed yellow emission in Mg_3N_2 .

DOI: [10.1103/PhysRevMaterials.4.064604](https://doi.org/10.1103/PhysRevMaterials.4.064604)

I. INTRODUCTION

The III-nitride semiconductors XN ($X = \text{Al}, \text{Ga}, \text{In}$) and their alloys [1–5] have important applications in many optoelectronic devices, such as the solid-state light-emitting diode (LED), for their good thermal stability and wide emission range from green to deep-ultraviolet region [6,7]. Recently, a II-nitride, Mg_3N_2 , has been demonstrated as a visible-light-emitting material that may find various optoelectronic applications [8–10]. Mg_3N_2 exhibits a broadband yellow-orange (~ 2 eV) photoluminescence (PL) emission upon excitation at 2.9 eV [8,10], which is close to the emission of a blue LED chip. The sub-band-gap PL is usually associated with deep electronic levels caused by permanent defects [11] or transient lattice distortions [12]. Nitrogen vacancy was suggested to be a likely source of the observed yellow PL [8,10]. The observed same excitation wavelength (420 nm) in three nitrides [8,10], Mg_3N_2 , CaMg_2N_2 , and Li_3AlN_2 , also suggest that it may originate from a common defect in the three nitrides, possibly the N vacancy. The self-activated luminescent materials as alternatives to rare-earth activated phosphors have a great significance for the solid-state lighting technologies. In addition to the interesting luminescent properties, Mg_3N_2 and related nitride compounds have also attracted considerable interests for their potential applications in reversible hydrogen storage materials [13–16] and high thermal conductivity ceramics [17].

Native defects and impurities play an important role in transport and optical properties of semiconductors. Extensive studies have been carried out to investigate the origins of defect-related PL emission in semiconductors, such as GaN [18,19], AlN [20], BN [21], and ZnO [22]. Taking GaN for

example, after much debate, the gallium vacancy complex $V_{\text{Ga}}\text{-O}_\text{N}$ is widely accepted to be the origin of the observed yellow luminescence (YL) [18,19]. Furthermore, Van de Walle and coworkers showed that C_N is a deep acceptor and may also act as another possible source of the YL by using hybrid functional calculations [23]. For AlN, Al vacancies contribute to the PL at 2.78 eV with an absorption peak at 3.4 eV, and the complexes consisting of an aluminum vacancy and oxygen impurities give rise to absorption peaked at 4.0 eV or higher and emission peaked at 3.2–3.5 eV depending on the oxygen concentration [20]. In ZnO, the PL properties of $V_{\text{Zn}}\text{-H}$ complex may explain the signals observed by optical studies of single-photon emitters in ZnO [22]. More recently, hexagonal BN (*h*-BN) has attracted much attention because its PL at 4.1 eV has been shown to exhibit single-photon emission [24]. As for its origin, theoretical calculations show that C_N may be one possibility while C_B is not [21].

Hybrid density functional theory plays an important role in identifying the mechanism of defect-related optical transitions [20,25,26]. The hybrid functional approach cannot only obtain accurate band structures of semiconductors, but also give a reliable description of the defect localization. However, to the best of our knowledge, the detailed theoretical studies of the mechanism of observed PL in Mg_3N_2 are still lacking. A previous density functional theory (DFT) study of Mg_3N_2 based on the generalized-gradient approximation, which has significant errors in the calculations of the band gap and defect levels, focused on formation energies of native defects and hydrogen with the goal of understanding the role of Mg_3N_2 (as an impurity phase in Mg-doped GaN) in the *p*-type conductivity of GaN:Mg [27]. The defect-related optical properties of Mg_3N_2 have not been calculated. In this paper, the intrinsic defects and impurities in Mg_3N_2 are investigated by the hybrid density functional approach to understand the origin of the broadband emission in Mg_3N_2 . The impurities studied in this work include hydrogen, oxygen, and carbon,

*hlshi@buaa.edu.cn

†mhdu@ornl.gov

which tend to be present in the growth environment. Furthermore, the complexes of these impurities and native defects are also investigated. The optical excitation and emission at defects, impurities, and defect-impurity complexes are studied in detail. Our results show that the N vacancy, V_N , is the main source of the observed broadband yellow luminescence, and C_N may also contribute to the yellow emission if present. Our comprehensive study of the formation of defects and impurities and their optical properties should be valuable to the design of broadband light-emitting materials with optimized properties for lighting applications.

II. METHODS

All our calculations of Mg_3N_2 were performed within the DFT framework using the Heyd-Scuseria-Ernzerhof (HSE) hybrid functional [28] as implemented in the Vienna *Ab initio* Simulation Package (VASP) code [29]. The mixing parameter for the nonlocal Hartree-Fock exchange is set to be 0.28 to reproduce the experimentally measured band gap of 2.85 eV [30,31]. The cutoff energy for the plane-wave basis was set at 550 eV and the atomic positions were fully relaxed until the residual forces were less than 0.01 eV/Å. We used a supercell (80 atoms if defect-free) containing two primitive cells and a $2 \times 2 \times 2$ k -point mesh for all defect calculations. Experimental lattice parameters (space group $Ia\bar{3}$, $a = b = c = 9.96$ Å, $\alpha = \beta = \gamma = 90^\circ$) were used [32]. Based on our tests using larger supercells, the errors in transition levels, excitation and emission energies are less than 0.1 eV. Our tests regarding optimized lattice constant of Mg_3N_2 also show that our results are almost unchanged.

For defect calculations, the formation energy of a defect α in the charge state q is given by

$$\Delta H(\varepsilon_f, \mu_\alpha) = E_q - E_H - \sum_\alpha n_\alpha (\mu_\alpha + \mu_\alpha^{\text{ref}}) + q(\varepsilon_{\text{VBM}} + \varepsilon_f), \quad (1)$$

where E_q is the total energy of the supercell containing defect in charge state q , and E_H is the total energy of the defect-free supercell. n_α is the number of atom that are added ($n > 0$) or removed ($n < 0$). μ_α represents the chemical potential for atomic species α , with reference to μ_α^{ref} , which is taken as the chemical potential of the atomic species in its elemental bulk form or in the gas-phase molecule. ε_{VBM} is the energy of the valence-band maximum (VBM) and ε_f is the Fermi energy relative to the VBM. Charge image and potential alignment corrections [33,34] are performed wherever appropriate.

The thermodynamic charge transition level of a defect, $\varepsilon(q/q')$, corresponding to the change in the most stable charge state of the defect between q and q' , is given by the Fermi level, at which the formation energies, $\Delta H(q)$ and $\Delta H(q')$, for charge states q and q' are equal to each other:

$$\varepsilon(q/q') = [\Delta H(q) - \Delta H(q')]/(q' - q). \quad (2)$$

The charge transition level of a defect due to optical transitions between the defect level and the conduction/valence band, $\varepsilon_{\text{opt}}(q/q')$, can also be calculated using the same method described above except that $\Delta H(q)$ and $\Delta H(q')$ should both be calculated using the relaxed defect structure before the

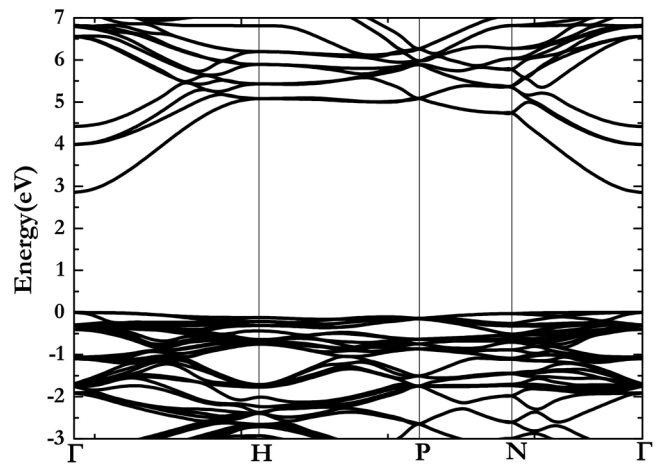


FIG. 1. Calculated band structure for Mg_3N_2 using the HSE hybrid functional.

optical transition. For example, for the excitation of an electron from a defect with the initial charge state of q to the conduction band minimum (CBM), the excitation energy is given by $E_g - \varepsilon_{\text{opt}}(q/q - 1)$; here, $\varepsilon_{\text{opt}}(q/q - 1)$ is calculated using the relaxed defect structure at the charge state q . For the subsequent radiative recombination, the emission energy is given by $E_g - \varepsilon_{\text{opt}}(q - 1/q)$; here, $\varepsilon_{\text{opt}}(q - 1/q)$ is calculated using the relaxed defect structure at the charge state $q - 1$.

In order to obtain the stable growth of Mg_3N_2 and avoid the undesirable formation of other competing phases, the chemical potentials μ_{Mg} and μ_N must meet the following conditions:

$$\begin{aligned} \mu_{\text{Mg}} &\leq 0 \\ \mu_N &\leq 0 \\ 3\mu_{\text{Mg}} + 2\mu_N &= \Delta H_f(Mg_3N_2) = -4.87 \text{ eV}, \end{aligned} \quad (3)$$

where $\Delta H_f(Mg_3N_2)$ is the heat of formation for Mg_3N_2 . Therefore, at the N-rich limit, $\mu_N = 0$ and $\mu_{\text{Mg}} = -1.62$ eV, while at the Mg-rich limit, $\mu_{\text{Mg}} = 0$ and $\mu_N = -2.44$ eV. The chemical potentials of H, O, and C are set to the energy per atom in the H_2 , O_2 diatomic molecules and the graphite, respectively.

III. RESULTS AND DISCUSSION

A. Electronic structures of Mg_3N_2

Our calculated band structure of Mg_3N_2 is shown in Fig. 1. Mg_3N_2 is a direct-gap semiconductor. The mixing parameter for nonlocal Hartree-Fock potential is set to be 0.28, resulting in a band gap of 2.85 eV that accords well with the experimental value [30,31]. The valence band has a mixing of flat and dispersive bands, which is mainly made up of N $2p$ states, while the conduction band is dispersive and consists of delocalized Mg s states.

B. Native point defects in Mg_3N_2

Six native point defects in Mg_3N_2 : two vacancy defects (V_N , V_{Mg}), two interstitial defects (N_i , Mg_i), and two antisite defects (Mg_N , N_{Mg}) are considered. The nitrogen vacancy is

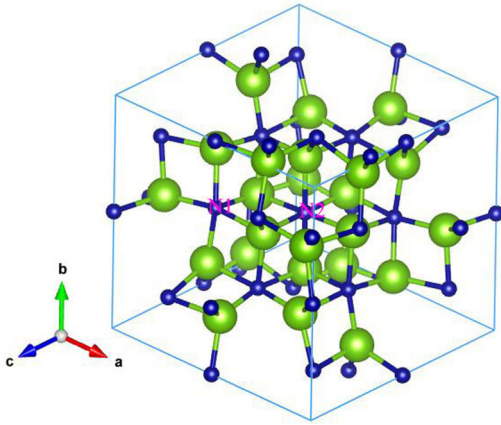


FIG. 2. The crystal structure of Mg_3N_2 . The two different N sites are marked.

extensively studied in nitrides because of its unique properties. In the following, our results also show that V_N plays a dominant role in the defect properties in Mg_3N_2 . There are two inequivalent N sites but just one Mg site in Mg_3N_2 as shown in Fig. 2. For the V_N defect, the energy difference

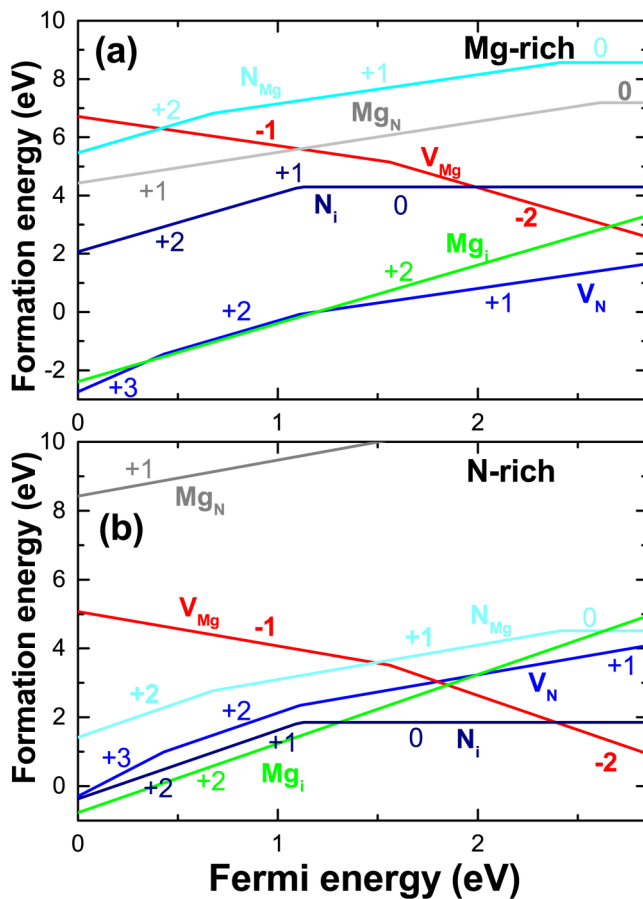


FIG. 3. Calculated formation energies of intrinsic defects as a function of the Fermi energy at (a) the Mg-rich limit and (b) the N-rich limit conditions. The slope of a formation energy line indicates the charge state of the defect. A charge transition level is the Fermi level at which the slope changes.

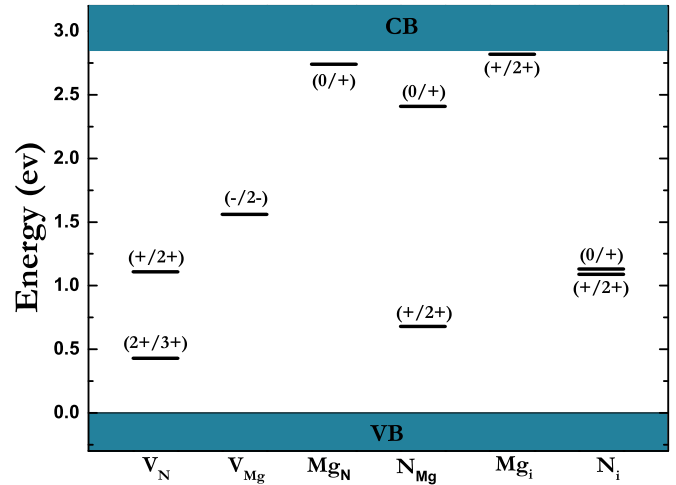


FIG. 4. Calculated thermodynamic charge transition levels for native defects in Mg_3N_2 . The energy of the VBM is set to zero.

between the two N sites is about 0.48 eV. Therefore, only the results based on the lower-energy N vacancy (N_2 site shown in Fig. 2) is presented below. Our calculated defect formation energies (as a function of the Fermi energy) and transition levels between different charge states are shown in Fig. 3 at Mg-rich and N-rich limits.

As shown in Fig. 3, the most important acceptor defect is V_{Mg} and the most important donor defects are Mg_i and V_N . Under the N-rich condition, N_i is also an important donor defect. Mg_i is a shallow donor while V_N and V_{Mg} are deep donor and acceptor defects, respectively. N_i is in the split-interstitial position, i.e., two N atoms occupy a N lattice site and form a N–N bond of 1.28 (1.39) Å at the + (neutral) state. Antisite defects show large formation energies under both N- and Mg-rich growth conditions, which may be expected because the large electronegativity difference between Mg and N makes the antisite defects difficult to form. At the Mg-rich limit [Fig. 3(a)], there are no native acceptors to compensate the native donor defect V_N . At the N-rich limit [Fig. 3(b)], the lowest-energy donor, Mg_i , and the lowest-energy acceptor, V_{Mg} , pin the Fermi level at the crossing point of their formation energy lines, which is above the midgap. Therefore, undoped Mg_3N_2 should be naturally *n* type.

Figure 4 presents our calculated transition energy levels of the above six native defects in Mg_3N_2 . V_N is a deep donor with deep transition levels, $(2+/3+)$ and $(+/2+)$, located at 0.43 and 1.11 eV above the VBM, respectively. In V_N^{3+} , the Mg cations adjacent to the vacancy repel each other, resulting in an increased Mg-vacancy distance of 2.50 Å. The addition of electrons into V_N^{3+} creates energy incentive for the Mg cations to move closer to each other; the resulting enhanced hybridization among the Mg *s* orbitals creates a bound state that traps the electrons. As a result, the Mg-vacancy distance is decreased from 2.50 Å in V_N^{3+} to 2.40 Å in V_N^{2+} , 2.28 Å in V_N^+ , and 2.23 Å for V_N^0 . For V_{Mg}^{2-} , the two electrons fill a single-particle level at about 0.23 eV above the VBM, while for V_{Mg}^- , the hole-occupied single-particle level is deep inside the band gap due to the hole polaron bound to V_{Mg} (see

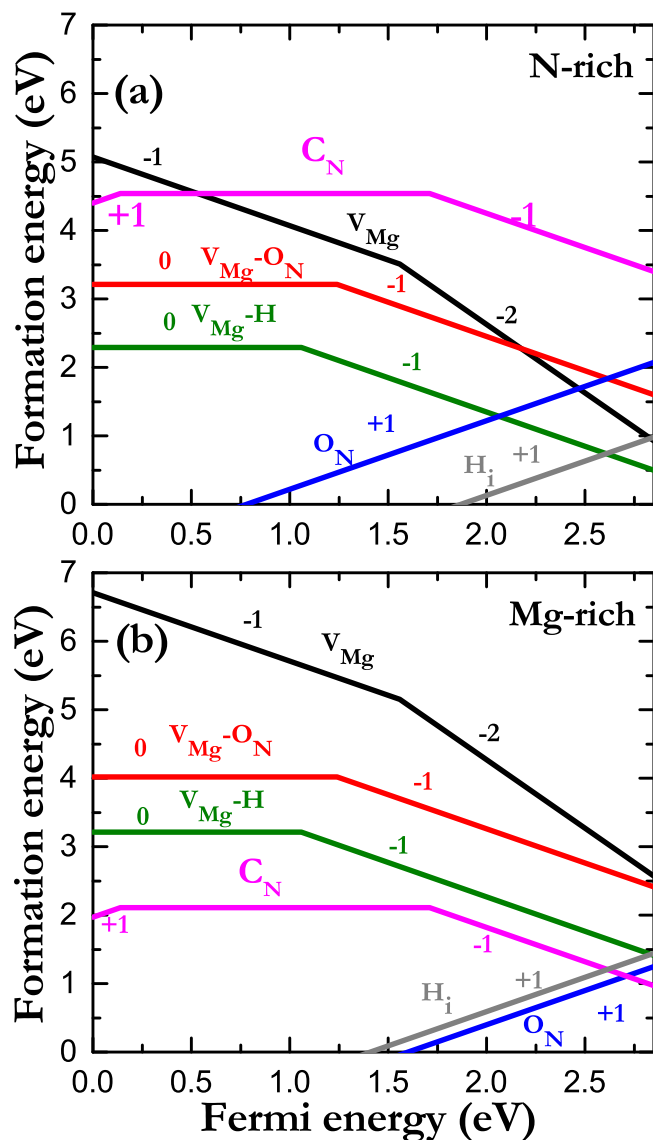


FIG. 5. Calculated formation energies of impurities in Mg_3N_2 as a function of Fermi level in N-rich and Mg-rich conditions for H, O, and C impurities and related complexes.

the charge densities in the Supplemental Material [35]). As a result, the $(-/2-)$ transition level is very deep, 1.6 eV above the VBM.

C. Impurities and related complex defects in Mg_3N_2

Unintentionally incorporated hydrogen, oxygen, and carbon are usually found in nitrides. These impurities also tend to bind with vacancies, forming complexes. The isolated H_i , O_N , and C_N impurities as well as the complexes with the vacancy, $\text{V}_{\text{Mg}}\text{-H}$ and $\text{V}_{\text{Mg}}\text{-O}_N$, are investigated. The calculated formation energies for the above defects are shown in Fig. 5.

H_i binds with a single N atom, forming a N-H bond with the bond length of 1.035 Å. H_i is a shallow donor and can bind strongly with the acceptor V_{Mg} .

The $\text{V}_{\text{Mg}}\text{-H}$ complex is a single-electron acceptor with its $(-/0)$ transition level located at 1.06 eV above the VBM, which is shallower than the $(2-/ -)$ level of isolated V_{Mg} . The

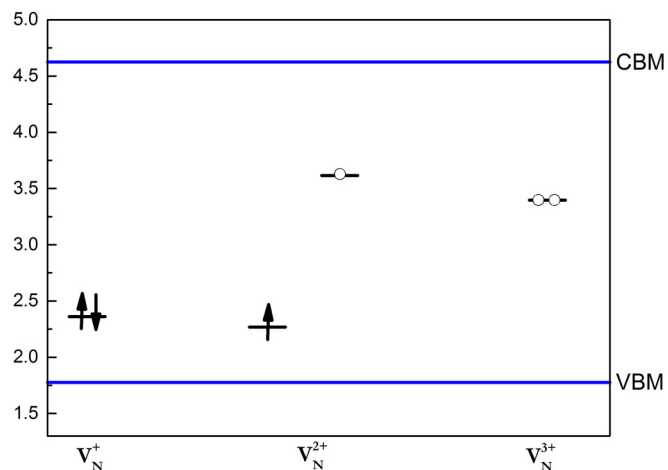


FIG. 6. Calculated single-electron levels of different charge states of V_N .

calculated binding energy between V_{Mg} and H_i is -1.43 eV, indicating strong binding (The binding energy is given by as $\Delta H[(\text{V}_{\text{Mg}} - \text{H})^-] - \Delta H(\text{V}_{\text{Mg}}^{2-}) - \Delta H(\text{H}_i^+)$).

O_N is a shallow donor with a low formation energy as shown in Fig. 4. O_N^+ can bind with $\text{V}_{\text{Mg}}^{2-}$ forming $(\text{V}_{\text{Mg}} - \text{O}_N)^-$ with the calculated binding energy -0.60 eV. $(\text{V}_{\text{Mg}} - \text{O}_N)^-$ acts as a deep acceptor, with $(-/0)$ transition level at 1.24 eV above the VBM. C_N is amphoteric with its $(0/+)$ and $(0/-)$ transition levels located at 0.14 and 1.71 eV, respectively, referenced to the VBM.

D. Optical transitions in Mg_3N_2

Based on the above defect calculations, the deep defects V_N , V_{Mg} , C_N , $\text{V}_{\text{Mg}}\text{-H}$, and $\text{V}_{\text{Mg}}\text{-O}_N$ are studied further for their optical properties, which may be related to the observed absorption and sub-band-gap emission peaks. N interstitial is not discussed further since our calculated emission of $\text{N}^+ + e^- \rightarrow \text{N}^0$ transition is only 1.2 eV, much smaller than the experimental value of 2.2 eV [10].

1. Isolated V_N and C_N defects

V_N (N_2 site shown in Fig. 2) introduces multiple defect states within the band gap. For neutral V_N , there are three electrons associated with the dangling bonds. According to symmetry analysis, V_N exhibits S_6 point symmetry. The defect states consist of A_g , A_u , and double-degenerate E_u states. Our results show that neutral V_N is metastable since the $(0/+)$ transition level is above CBM. For V_N^+ and V_N^{2+} , two and one electrons occupy the A_g state, respectively, while for V_N^{3+} , A_g states are empty. For these three charged V_N states, A_u and E_u are empty and resonant in the conduction bands. To show the defect states more clearly, our calculated single-electron levels for charged V_N are showed in Fig. 6.

According to above discussions, there are many possible optical excitations at V_N , including the excitation of an electron from V_N^{2+} or V_N^+ to the CBM $[(\text{V}_N^{2+} \rightarrow \text{V}_N^{3+} + e^-)$ or $(\text{V}_N^+ \rightarrow \text{V}_N^{2+} + e^-)]$. The reverse of the above excitations leads to emissions of various emission energies. Figure 7 presents a configuration coordinate diagram for various

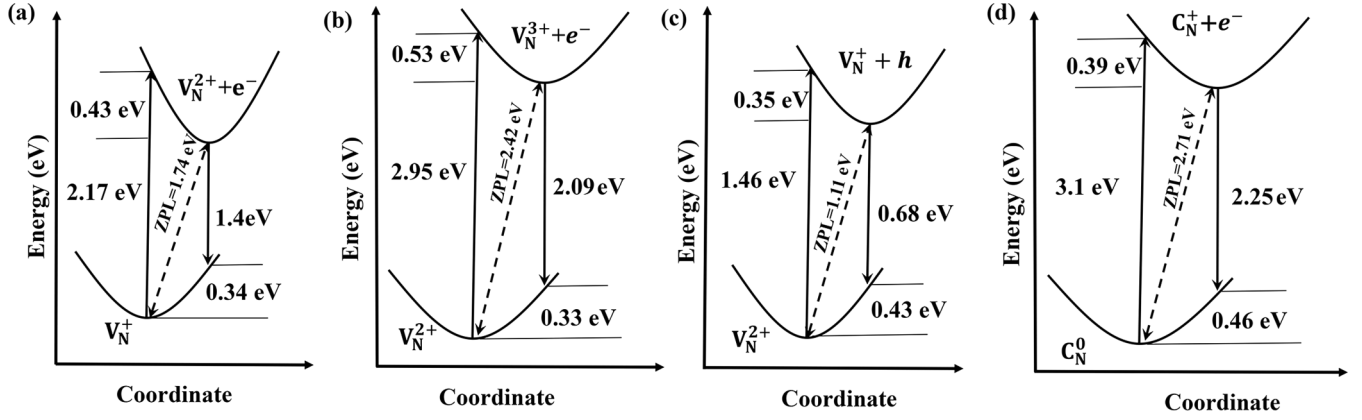


FIG. 7. Schematic configuration coordinate diagrams for optical transitions associated with the (a) V_N (+/2+) level exchanging an electron with the CBM, (b) V_N (2+/3+) level exchanging an electron with the CBM, (c) V_N (+/2+) level exchanging a hole with VBM, (d) C_N (0/+1) level exchanging an electron with CBM.

optical transitions associated with V_N . For $V_N^{+} \rightarrow V_N^{2+} + e^-$ transition [Fig. 7(a)], the electron is excited from V_N^{+} to the CBM, the excitation energy corresponding to the peak of absorption is calculated to be 2.17 eV (vertical transition in classical approximation). For the subsequent recombination process $V_N^{2+} + e^- \rightarrow V_N^{+}$, the emission is peaked at 1.4 eV with a zero-phonon line (ZPL) of 1.74 eV. The excitation of an electron from V_N^{2+} to the CBM [$V_N^{2+} \rightarrow V_N^{3+} + e^-$, Fig. 7(b)] requires the excitation energies of 2.95 eV; the subsequent recombination leads to emissions at 2.09 eV, which are in good agreement with the experimentally observed PL peak at 2.20 eV [8,10].

The optical process that excites electrons from the VBM to the defect state of V_N^{2+} is also considered, forming excited state $V_N^{+} + h$. Our calculated excitation energy is 1.46 eV, and the emission energy is only 0.68 eV [shown in Fig. 7(c)]. Nonradiative instead of radiative process is much more likely to occur at such low emission energies since typical non-radiative capture coefficients are much larger than radiative coefficients for carriers recombination at these low energies [22,36–38].

The above results suggest that V_N may be responsible for the experimentally observed yellow-orange emission [8,10]. V_N may be directly excited [e.g., $V_N^{2+} \rightarrow V_N^{3+} + e^-$, Fig. 7(b)]. The strong excited-state structural relaxation as shown by the configuration coordinate diagrams in Fig. 7 also suggests significant electron-phonon coupling and broad emissions.

Electron paramagnetic resonance (EPR) can help to detect nitrogen vacancy centers. According to our above intrinsic defect discussions, undoped Mg_3N_2 should be naturally n typed. V_N^{+} should be stable and electrons occupy A_g state paired off. Therefore, V_N^{+} is nonmagnetic and no EPR is observed. If the Mg_3N_2 sample is irradiated by electron or other methods, the electron is pumped from V_N^{+} and V_N^{2+} is formed. The spin state of V_N^{2+} is $S = 1/2$ and therefore the defect center maybe detectable. For V_N^{3+} , no electrons occupy the defect levels and electrons are paired off, the defect are nonparamagnetic, and no EPR is observed.

For the C_N center, starting from the initial state of C_N^0 , an electron is excited to the CBM and C_N^{+} is formed, shown in Fig. 7(d). Our predicted excitation energy and emission

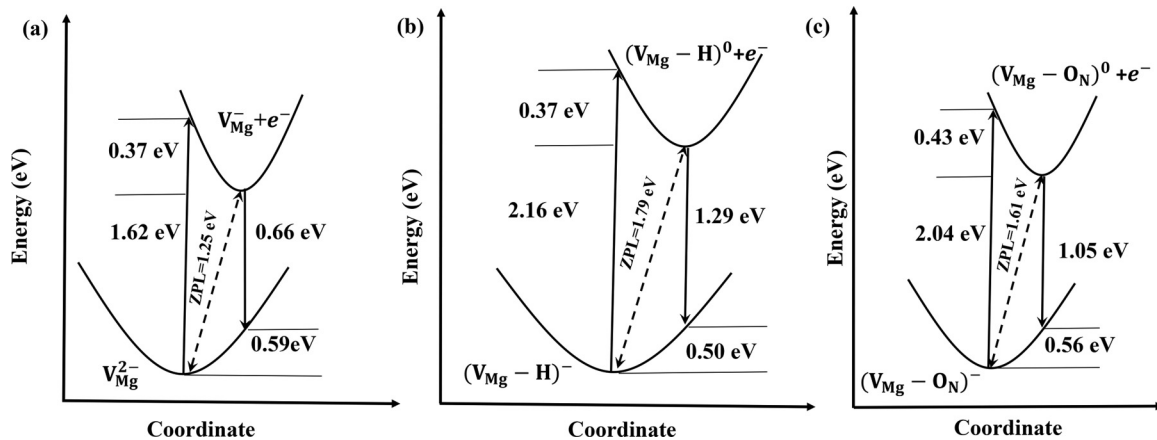


FIG. 8. Schematic configuration coordinate diagrams for optical transitions associated with the (a) V_{Mg} (2-/1-) level exchanging an electron with CBM, (b) $V_{Mg}-H$ (-/0) level exchanging an electron with the CBM, (c) $V_{Mg}-O_N$ (-/0) level exchanging an electron with the CBM.

energy are 3.1 and 2.25 eV, respectively, which are in good agreement with experimental values [8,10]. Its ZPL of 2.71 eV is also consistent very well with the excitation onset near 450 nm [8,10]. These results suggest that C_N , if present in the sample, could also contribute to the observed broadband emission.

2. Isolated V_{Mg} and complexes of V_{Mg} -H and V_{Mg} - O_N

The optical transition for $V_{Mg}^{2-} \rightarrow V_{Mg}^{-} + e^{-}$ is shown in Fig. 8(a). Our calculated excitation energy is 1.62 eV and emission energy is 0.66 eV, which should be a nonradiative process as discussed before. Figure 8(b) shows the optical transition of $(V_{Mg} - H)^{-} \rightarrow (V_{Mg} - H)^0 + e^{-}$ in Mg_3N_2 with the calculated excitation peak at 2.16 eV and emission peak at 1.29 eV. Figure 8(c) shows the transitions associated with the V_{Mg} - O_N complex. The electron at $(V_{Mg}-O_N)^{-}$ is excited to the CBM with an excitation energy of 2.04 eV. The recombination between the electron at CBM and hole at the defect state gives rise to an emission at 1.05 eV. The above-calculated emission energies by V_{Mg} as well as V_{Mg} complexed with H and O impurities do not agree with the experimentally observed PL energies [8,10].

IV. CONCLUSION

Hybrid functional calculations are performed to calculate the formation energies and optical transition energies of native defects, common impurities (H, O, and C), and defect-impurity complexes in Mg_3N_2 . V_N and V_{Mg} are found to

be important donor and acceptor defects and both introduce deep levels in the band gap of Mg_3N_2 . H_i and O_N act as shallow donors while C_N is amphoteric. The binding of the V_{Mg} acceptor with H and O donors form stable complexes of V_{Mg} -H and V_{Mg} - O_N with shallower transition levels compared to isolated V_{Mg} . The calculated optical transition energies suggest that V_N and C_N are two possible sources for the observed broad yellow-orange PL.

ACKNOWLEDGMENTS

H. Shi was supported by the National Natural Science Foundation of China (NSFC) under Grant No.11604007 and the start-up funding at Beihang University. The work at ORNL were supported by the U.S. Department of Energy, Office of Science, Basic Energy Sciences, Materials Sciences and Engineering Division.

This work has been partially supported by UT-Battelle, LLC under Contract No. DE-AC05-00OR22725 with the U.S. Department of Energy. The United States Government retains and the publisher, by accepting the article for publication, acknowledges that the United States Government retains a non-exclusive, paid-up, irrevocable, world-wide license to publish or reproduce the published form of this manuscript, or allow others to do so, for United States Government purposes. The Department of Energy will provide public access to these results of federally sponsored research in accordance with the DOE Public Access Plan (<https://energy.gov/downloads/oe-public-access-plan>).

- [1] J. S. Harris, B. E. Gaddy, R. Collazo, Z. Sitar, and D. L. Irving, *Phys. Rev. Mater.* **3**, 54604 (2019).
- [2] P. Deák, M. Lorke, B. Aradi, and T. Frauenheim, *Phys. Rev. B* **99**, 085206 (2019).
- [3] P. Vennegues, M. Benaissa, B. Beaumont, E. Feltin, P. D. Mierry, S. Dalmaso, M. Leroux, and P. Gibart, *Appl. Phys. Lett.* **77**, 880 (2000).
- [4] M. Hansen, L. F. Chen, S. H. Lim, S. P. Denbaars, and J. S. Speck, *Appl. Phys. Lett.* **80**, 2469 (2002).
- [5] P. Vennéguès, M. Leroux, S. Dalmaso, M. Benaissa, P. De Mierry, P. Lorenzini, B. Damilano, B. Beaumont, J. Massies, and P. Gibart, *Phys. Rev. B* **68**, 235214 (2003).
- [6] F. A. Ponce and D. P. Bour, *Nature (London)* **386**, 351 (1997).
- [7] J. Neugebauer and C. G. Van de Walle, *Appl. Phys. Lett.* **68**, 1829 (1996).
- [8] B. Ma, J. Ding, Q. Long, and Y. Wang, *J. Lumin.* **208**, 388 (2019).
- [9] X. J. Wang, S. Funahashi, T. Takeda, T. Suehiro, N. Hirosaki, and R. J. Xie, *J. Mater. Chem. C* **4**, 9968 (2016).
- [10] Y. Uenaka and T. Uchino, *J. Phys. Chem. C* **118**, 11895 (2014).
- [11] C. Freysoldt, B. Grabowski, T. Hickel, J. Neugebauer, G. Kresse, A. Janotti, and C. G. Van de Walle, *Rev. Mod. Phys.* **86**, 253 (2014).
- [12] M. D. Smith and H. I. Karunadasa, *Acc. Chem. Res.* **51**, 619 (2018).
- [13] Y. Kojima, Y. Kawai, and N. Ohba, *J. Power Sources* **159**, 81 (2006).
- [14] Y. Nakamori, G. Kitahara, K. Miwa, S. Towata, and S. Orimo, *Appl. Phys. A: Mater.* **80**, 1 (2005).
- [15] C. Ping, X. Zhitao, L. Jizhong, L. Jianyi, and T. Kuang Lee, *Nature (London)* **420**, 302 (2002).
- [16] J. Lu, Z. Z. Fang, Y. J. Choi, and Y. S. Hong, *J. Phys. Chem. C* **111**, 12129 (2007).
- [17] Z. Lenčič, K. Hirao, Y. Yamauchi, and S. Kanzaki, *J. Am. Ceram. Soc.* **86**, 1088 (2004).
- [18] R. Armitage, W. Hong, Q. Yang, H. Feick, J. Gebauer, E. R. Weber, S. Hautakangas, and K. Saarinen, *Appl. Phys. Lett.* **82**, 3457 (2003).
- [19] A. Sedhain, J. Li, J. Y. Lin, and H. X. Jiang, *Appl. Phys. Lett.* **96**, 151902 (2010).
- [20] Q. Yan, A. Janotti, M. Scheffler, and C. G. Van de Walle, *Appl. Phys. Lett.* **105**, 111104 (2014).
- [21] L. Weston, D. Wickramaratne, M. Mackoit, A. Alkauskas, and C. G. Van de Walle, *Phys. Rev. B* **97**, 214104 (2018).
- [22] J. L. Lyons, J. B. Varley, D. Steiauf, A. Janotti, and C. G. Van de Walle, *J. Appl. Phys.* **122**, 035704 (2017).
- [23] J. L. Lyons, A. Janotti, and C. G. Van de Walle, *Appl. Phys. Lett.* **97**, 152108 (2010).
- [24] R. Bourrellier, S. Meuret, A. Tararan, O. Stă Phan, M. Kociak, L. H. Tizei, and A. Zobelli, *Nano Lett.* **16**, 4317 (2016).
- [25] C. G. Van de Walle, J. L. Lyons, and A. Janotti, *Phys. Status Solidi* **207**, 1024 (2010).
- [26] J. L. Lyons and C. G. Van de Walle, *NPJ Comp. Mater.* **3**, 1 (2017).

- [27] B. Lange, C. Freysoldt, and J. Neugebauer, *Phys. Rev. B* **81**, 224109 (2010).
- [28] J. Heyd and G. E. Scuseria, *J. Chem. Phys.* **118**, 8207 (2003).
- [29] G. Kresse and J. Furthmüller, *Phys. Rev. B* **54**, 11169 (1996).
- [30] K. Toyoura, T. Goto, H. Kan, and R. Hagiwara, *Electrochim. Acta* **51**, 56 (2005).
- [31] P. John, H. Rotella, C. Deparis, G. Monge, F. Georgi, P. Vennéguès, M. Leroux, and J. Zuniga-Perez, *Phys. Rev. Mater.* **4**, 054601 (2020).
- [32] D. E. Partin, D. J. Williams, and M. O’Keeffe, *J. Solid State Chem.* **132**, 56 (1997).
- [33] C. Freysoldt, J. Neugebauer, and C. G. Van de Walle, *Phys. Rev. Lett.* **102**, 016402 (2009).
- [34] C. Freysoldt, J. Neugebauer, and C. G. Van de Walle, *Phys. Status Solidi* **248**, 1067 (2011).
- [35] See Supplemental Material at <http://link.aps.org/supplemental/10.1103/PhysRevMaterials.4.064604> for charge densities for the highest occupied electron in -2 state of vacancy Mg and the hole bound to -1 state of vacancy Mg.
- [36] M. A. Reshchikov, *AIP Conf. Proc.* **1583**, 127 (2014).
- [37] D. Wickramaratne, J.-X. Shen, A. Alkauskas, and D. W. C. G. Van, *Phys. Rev. B* **97**, 077301 (2018).
- [38] C. E. Dreyer, A. Alkauskas, J. L. Lyons, J. S. Speck, and C. G. Van de Walle, *Appl. Phys. Lett.* **108**, 141101 (2016).